

# Permanent magnet working point ripple in synchronous generators

Stefan Sjökvist, Morgan Rossander, Sandra Eriksson

Division of Electricity, Department of Engineering Sciences, Uppsala University, Box 534, 75121 Uppsala, Sweden  
E-mail: morgan.rossander@angstrom.uu.se

Published in *The Journal of Engineering*; Received on 30th October 2016; Accepted on 24th March 2017

**Abstract:** Permanent magnets (PMs) are today widely used in electrical machines of all sorts. With their increase in popularity, the amount of research has increased as well. In this study, the magnetic flux density ripple of the working point of the PMs in a 100 kW PM synchronous generator has been investigated for three different load cases: no load, AC load, and DC load. The PMs will be subjected to a shift in working point as a consequence of the characteristics of the electrical loading. This study is based on finite element method simulations where the ripple of the magnetic flux density in the PMs was recorded at three positions within a PM. The slot harmonic of 7.5 times the electrical frequency ( $f_{el}$ ) was present in the results for all load cases, but mainly at the surface of the PM, as expected. Results showed an unexpected harmonic of  $1.5f_{el}$ , assumed to be an undertone of the slot harmonics. The  $6f_{el}$  harmonic for the DC load case was significantly higher than for the AC load case and is caused by the current fluctuation during passive rectification. For the studied machine, the added harmonics in the magnetic field due to passive rectification are less than the slot-related harmonics.

## 1 Introduction

Permanent magnet synchronous generators (PMSGs) are commonly used for renewable energy conversion [1]. One solution for the electrical system is passive rectification using diodes connected to a DC bus and an inverter [2]. The most damaging situations for PMs are short circuits. In normal operation, the magnets will be subjected to different magnetic loading depending on the electrical loading, causing a shift in working point for the magnets. The working point (or operating point) for a magnet is defined as its position on the  $B$ - $H$ -curve, i.e. the current values of the magnetic flux density ( $B$ ) and magnetic field ( $H$ ). It is important to determine the working point since a working point too far left on the  $B$ - $H$ -curve, in some part of the magnet, can cause partial demagnetisation. In addition, the working point ripple might cause eddy currents. In this paper, the working point and in particular the ripple of the working point for the PMs in a PMSG is studied for three different load cases: no load, a purely resistive AC load, and a diode-rectified DC load. The working point ripple is investigated at three different positions in the magnet, and an average working point ripple is calculated for all mesh points in the magnet. A frequency analysis is performed to study how the frequency content differs at the different positions in the magnets and for the various load cases. Finally, eddy current losses in the magnets are discussed.

A demagnetisation model for studying partial demagnetisation in PMs has been developed in-house and has been experimentally verified [3, 4]. For the work presented in this paper, the model has been extended with an external electrical circuit. In [5], the variation of the magnetic flux density at different points in a magnet was investigated during a short-circuit event and segmentation of the magnet was proposed as a mean to limit demagnetisation. A dual winding machine topology with separate rectifiers in series was suggested to reduce eddy current losses in diode-rectified PM machines in [6]. For machines with active rectification, the rotor is subject to much higher frequencies and the rotor losses needs to be more carefully investigated [7].

Eddy currents in PM machines have been studied in [8], where Polinder presented a method of equivalent circuits representing eddy current losses in a high-speed PM machine.

## 2 Study

The study includes a 100 kW generator which is an upscale version of a 12 kW generator previously studied [9, 10]. The PMs are

surface mounted, uniformly magnetised neodymium iron boron (NdFeB) magnets. Table 1 presents the main properties of the generator and information about the different load cases investigated. All cases were simulated at a temperature of 60°C. During the AC and DC load conditions, the same output power was delivered to the resistive load. The magnetic flux density was recorded at three positions within one PM as well as for the average of the whole PM. These positions denoted as A, B, and C were chosen along a line 1 mm below the surface of the magnet. Positions A and C are each 1 mm from the respective side of the PM, whereas B is positioned in the middle of the PM, as shown in Fig. 1. The average value of the PM is referred to as Avg. This figure shows one-fourth of the simulated geometry which represents the smallest symmetrical piece. The smallest symmetrical piece is one-eleventh of the whole geometry.

The study was conducted using the commercially available finite element method (FEM) software COMSOL Multiphysics [COMSOL Multiphysics is a registered trademark of COMSOL AB.], and all simulations were performed in two-dimensional (2D). Any 3D effects such as axial leakage flux and coil end impedances were neglected, e.g. the internal resistance of the generators would be slightly too low since the total length of the winding is underestimated due to the neglected coil ends. However, this will have a small impact on the results since the internal resistance is much lower than the resistance of the load. Eddy currents were calculated with the FEM software, but should be considered to be an approximation due to the 2D simulation.

### 2.1 Electric circuits

The AC circuit consists of a Y-connected resistive load connected directly to the generator output. Fig. 2 shows a schematic figure over the circuit used in the DC load case. The capacitance on the DC link for the DC load case was chosen large enough for the voltage ripple to be small, while still being somewhat realistic. As long as the capacitance value is high enough, the actual value is non-critical for the current fluctuations [11]. The chosen value of 50.0 mF resulted in a total peak-to-peak voltage ripple of <0.1%. For the generator to deliver the same power into the resistive load in both load cases, the resistive load was adjusted until the output power was  $100 \pm 0.1$  kW. The corresponding loads are presented in Table 1.

The rectifying bridge in the DC circuit, however, needed to be somewhat modified to get the FEM model to converge.

**Table 1** Basic geometrical and electrical properties of the 100 kW PMSG used in the study. The electrical properties are given at an operational temperature of 60°C

Power, kW	100
Phase voltage, no load, rms, V	296.2
Phase voltage, AC load, rms, V	278.1
Phase current, AC load, rms, A	119.9
Resistive load, $R_{AC}$ , AC case, $\Omega$	2.32
Phase voltage, DC load, rms, V	268.2
Phase current, DC load, rms, A	133.4
Resistive load, $R_L$ , DC case, $\Omega$	3.35
Capacitance, $C_{DC}$ , mF	50.0
Electrical frequency, $f_{el}$ , Hz	18.3
Rotational speed, rpm	50
Pole pairs	22
Slots per pole and phase	5/4
Stator length, mm	720
Stator radius (in/out), mm	600/720
Air gap, mm	8
PM height, mm	12

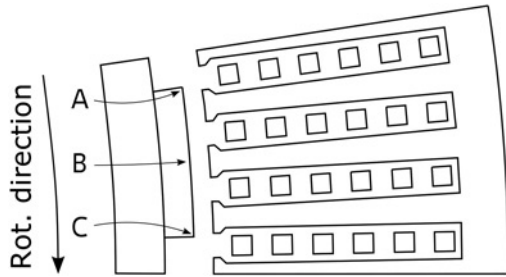


**Fig. 1** Cross-section of one-fourth of the geometry simulated. The left part is the rotor and the right part is the stator. The rotor consists of the PM (closest to the air gap) placed on an iron ring. The positions A, B, and C are positioned along a line 1 mm below the surface of the magnet. A and B are each 1 mm from the respective side, and B is placed in the middle of the PM. The rotational direction of the rotor is clockwise

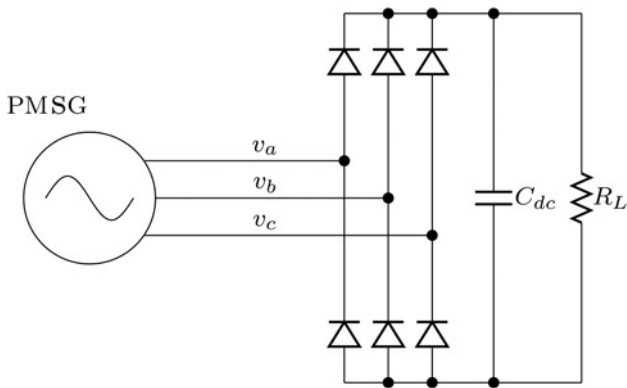


**Fig. 2** Schematic figure of the DC rectification circuit, in the simulations each diode was substituted with a VCCS and a snubber resistance, according to Fig. 3

The diodes were replaced with voltage controlled current sources (VCCSs) and snubber resistances ( $R_s$ ), as shown in Fig. 3. The VCCSs were controlled by the diode law

$$I_D = I_S (e^{(V_D/nV_T)} - 1) \quad (1)$$

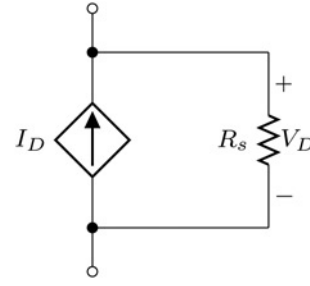


**Fig. 3** VCCS and  $R_s$  replaced each diode in the DC circuit

where  $I_D$  is the diode current,  $V_D$  is the voltage across the diode,  $I_S$  is the reverse bias saturation current,  $n$  is the ideality factor (1.25 in this case), and  $V_T$  is the thermal voltage. The thermal voltage is defined as

$$V_T = \frac{kT}{q} \quad (2)$$

where  $k$  is the Boltzmann constant,  $T$  is the absolute temperature, and  $q$  is the magnitude of the charge of an electron. The snubber resistances were added for one reason; in the FEM software,  $V_D$  had to be measured over  $R_s$  not to cause a circular dependency. As a compromise between the leakage current through  $R_s$  and the stability of the simulation,  $R_s$  was set to 10 k $\Omega$ .

## 2.2 Frequency analysis

The simulations are performed for a duration of two electrical periods plus settling time to stabilise the model. The time step of the simulations is 0.01 ms. The two electrical periods obtained from the FEM simulations are repeated 100 times before performing a fast Fourier transform (FFT) with a minimum 4-term Blackman–Harris window.

The obtained FFT amplitude is scaled by its average according to

$$\frac{\text{fft}(x)}{\langle x \rangle} = \frac{\text{fft}(x)}{\text{fft}(x)|_{\omega=0}} \quad (3)$$

We denote this scaled FFT as the *relative spectral amplitude*. The frequency vector is scaled to the electrical frequency ( $f_{el}$ ), giving the harmonics as order,  $n$ , of the electrical frequency,  $n f_{el}$ .

## 3 Results and discussion

The working point does not change much for the different loading cases. However, the corner of the magnet, point C is more affected by the loading than the average for the whole magnet, Avg. The change in the minimum value of the magnetic flux density at position C and the Avg. for the different load cases are presented in a  $B$ – $H$ -curve in Fig. 4. The ripple of the magnetic flux density for all three load cases is presented in Fig. 5. The magnetic flux density in the no load case at positions A and C (the corners) have almost the same amplitude, as expected for a uniformly magnetised magnet, but are phase shifted due to the stator teeth alignment. In the AC and DC load cases, the magnetic flux density at position A has somewhat increased due to the load angle and the rotational direction. The trailing corner, A, will experience a rise in the magnetic flux density, whereas the leading corner, C, will experience a decrease in magnetic flux density. In the AC load case, the voltage and current in the generator are almost sinusoidal. However, when the generator is connected to a rectifier and a DC load, the voltage and current waveforms will be distorted and therefore contain harmonics, see Fig. 6.

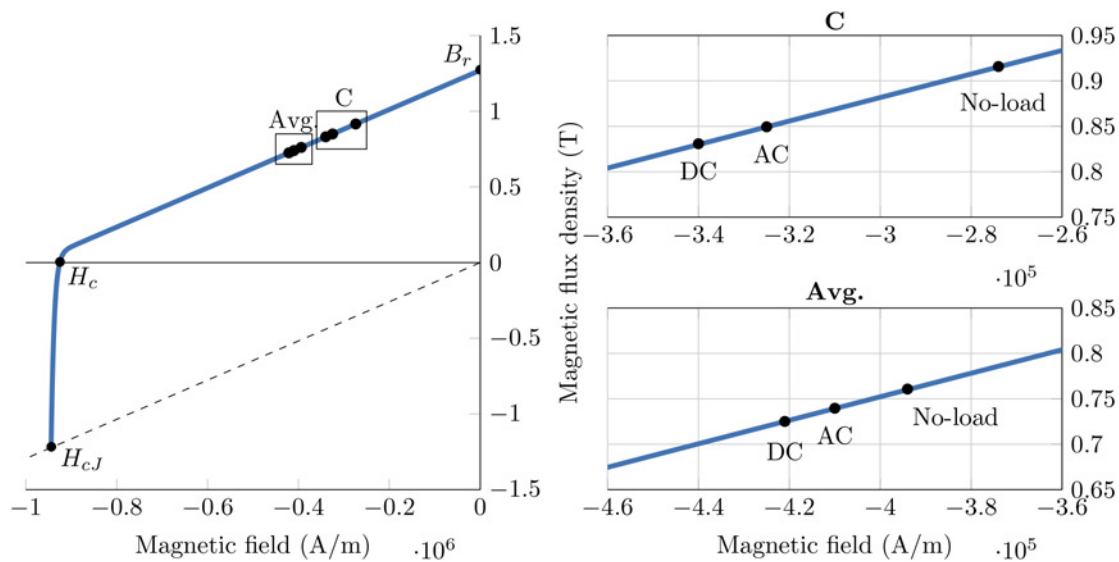


**Fig. 4** Minimum value of magnetic flux density ripple at position C and the average of the PM (Avg.) during the different load cases at 60°C

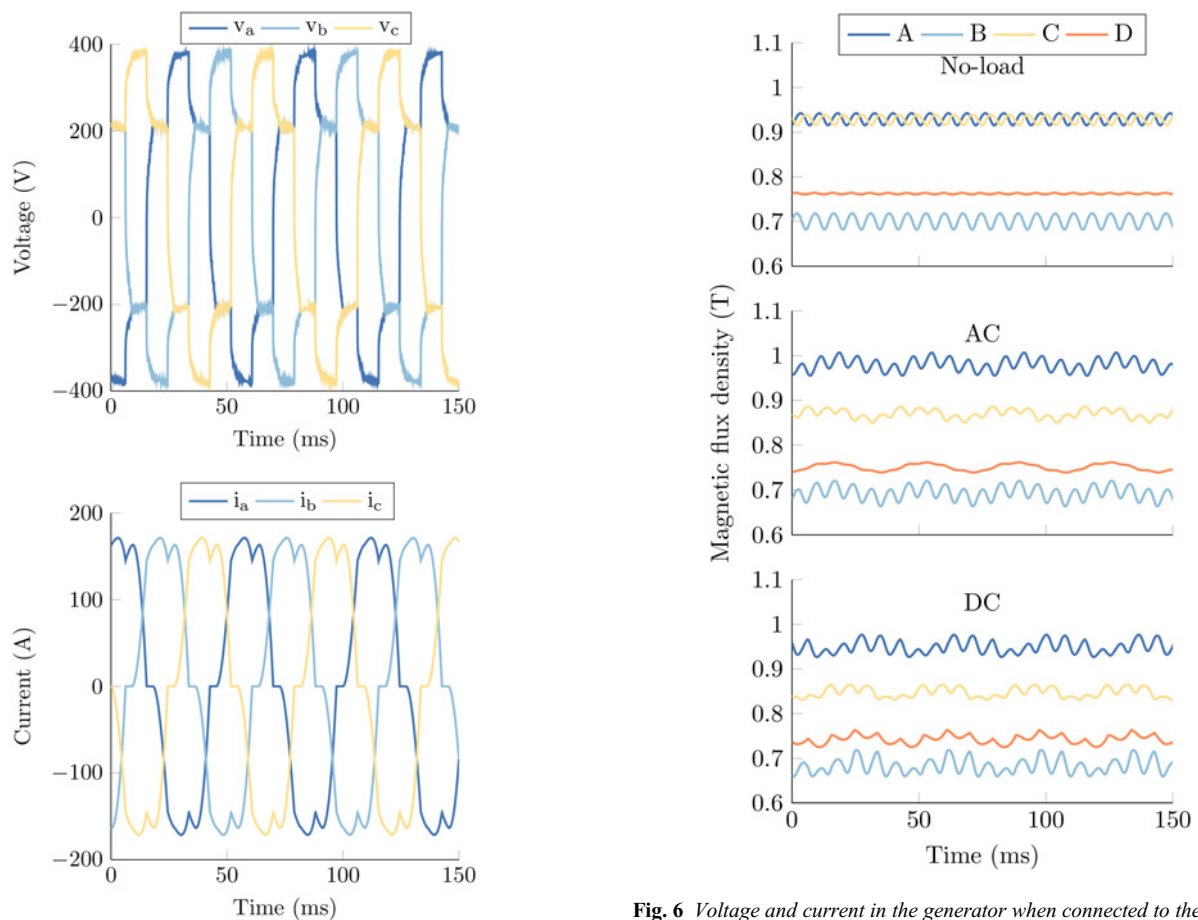


**Fig. 5** Magnetic flux density ripple at the different positions in the PM during no load, AC load, and a DC load case at 60°C

The result of the frequency analysis of the results in Fig. 5 is presented in Table 2. The harmonic content is different for the different loading cases and the different points in the magnet. The slot harmonic at  $7.5f_{el}$  is present in all load cases, but mainly on the surface of the magnet. The  $6f_{el}$  DC harmonic affects the whole magnet. An unexpected harmonic at  $1.5f_{el}$  was found, and it seems to increase with increasing load. It did not seem to result

**Fig. 6** Voltage and current in the generator when connected to the rectifier and DC load

from any harmonic in the electrical current. Therefore, it was assumed that this harmonic is a result from the magnet only covering part of the pole pitch, leaving some teeth (one out of fifth) with very low electromagnetic flux density at a certain position, i.e. giving an undertone of the slot harmonic. The increase at higher load is probably due to the increasing load angle. The small harmonics at 3, 4.5, and (for the AC load case)  $6f_{el}$  are also assumed to be a consequence of the slotting. The  $6f_{el}$  harmonic in the DC load case is significantly higher than the AC load case. The  $6f_{el}$  harmonic is

**Table 2** Result of the frequency of the magnetic flux density at the different positions within the PM. The presented values are the relative spectral amplitudes in percentage

Case	Position	$0.5f_{el}$	$1.5f_{el}$	$3f_{el}$	$4.5f_{el}$	$6f_{el}$	$7.5f_{el}$	$12f_{el}$	$14f_{el}$	$15f_{el}$
no load	A	0.00	0.00	0.00	0.00	0.00	1.41	0.00	0.00	0.11
	B	0.00	0.16	0.01	0.01	0.00	2.52	0.00	0.00	0.18
	C	0.00	0.00	0.00	0.00	0.00	1.21	0.00	0.00	0.11
	Avg.	0.00	0.14	0.01	0.01	0.00	0.21	0.00	0.00	0.00
AC load	A	0.00	1.06	0.22	0.17	0.08	1.55	0.01	0.01	0.11
	B	0.01	1.49	0.14	0.03	0.02	2.56	0.00	0.00	0.19
	C	0.00	1.18	0.30	0.29	0.04	0.92	0.01	0.00	0.12
	Avg.	0.01	1.36	0.07	0.09	0.01	0.16	0.00	0.00	0.00
DC load	A	0.00	1.22	0.24	0.14	0.66	1.51	0.08	0.02	0.12
	B	0.01	1.64	0.18	0.17	1.54	2.47	0.24	0.02	0.19
	C	0.00	1.41	0.35	0.32	0.49	0.90	0.05	0.08	0.13
	Avg.	0.01	1.46	0.09	0.23	1.07	0.14	0.18	0.02	0.00

caused by the current fluctuation during the passive rectification, and it can be significant. In the original 12 kW machine, the fluctuation in electric torque at nominal power was determined to be in the range of 20–30% [11]. For the machine considered here, the torque ripple is only 6%, and the resulting field ripple is at most 1.54% for the studied positions. The reason for the lower torque ripple in the 100 kW machine is the higher current in combination with the larger generator inductance, compared with the 12 kW machine.

An approximation of the eddy current losses from the 2D simulations suggests that the eddy current losses in the DC load case is about 2.5 times higher than in the AC load case, caused by the increase in the  $6f_{el}$  harmonic. However, for both cases the eddy current losses are very low. The eddy current losses are calculated from the 2D simulations by the FEM software. Since the eddy currents mainly flow in the out-of-plane direction, further research and 3D simulations are required to determine the eddy current losses with accuracy. The 3D effect on the eddy current losses are expected to affect the AC and DC case in a similar way, i.e. the relative difference between the losses stating that the eddy current losses are higher at DC load, should be valid.

#### 4 Conclusion

The change in working point for different load cases turned out to be small. However, the working point ripple was different for different load conditions. For the studied machine, the added harmonics in the magnetic field due to passive rectification, i.e. the 6th harmonic, are less than the presumably slot-related harmonics at  $1.5f_{el}$ . However, the harmonics from the passive rectification have a higher frequency and will, therefore, cause more eddy current losses.

#### 5 Acknowledgments

This work was carried out with funding from the Swedish Research Council, grant number 2010-3950 and within the STandUP for Energy strategic research framework. The Åforsk Foundation grant number 12-295 and Carl Trygger's Foundation, grant number 15:152 is also acknowledged for contributing to this work.

#### 6 References

- [1] Chen Y., Pillay P., Khan A.: 'PM wind generator topologies', *IEEE Trans. Ind. Appl.*, 2005, **41**, (6), pp. 1619–1626, doi: 10.1109/TIA.2005.858261
- [2] Apelfröjd S., Eriksson S., Bernhoff H.: 'A review of research on large scale modern vertical axis wind turbines at Uppsala University', *Energies*, 2016, **9**, (7), p. 570, doi: 10.3390/en9070570
- [3] Sjökvist S., Eriksson S.: 'Experimental verification of a simulation model for partial demagnetization of permanent magnets', *IEEE Trans. Magn.*, 2014, **50**, (12), pp. 1–5, doi: 10.1109/TMAG.2014.2339795
- [4] Sjökvist S., Eklund P., Eriksson S.: 'Determining demagnetisation risk for two PM wind power generators with different PM material and identical stators', *IET Electr. Power Appl.*, 2016, **10**, (7), pp. 593–597, doi: 10.1049/iet-epa.2015.0518
- [5] McFarland J.D., Jahns T.M.: 'Investigation of the rotor demagnetization characteristics of interior PM synchronous machines during fault conditions', *IEEE Trans. Ind. Appl.*, 2014, **50**, (4), pp. 2768–2775, doi: 10.1109/TIA.2013.2294997
- [6] Qazalbash A., Sharkh S.M., Irenji N.T., *ET AL.*: 'Rotor eddy current power loss in permanent magnet synchronous generators feeding uncontrolled rectifier loads', *IEEE Trans. Magn.*, 2014, **50**, (6), pp. 1–11, doi: 10.1109/TMAG.2013.2297391
- [7] de Santiago J., Oliveira J.G., Bernhoff H.: 'Filter influence on rotor losses in coreless axial flux permanent magnet machines', *Adv. Electr. Comput. Eng.*, 2013, **13**, (1), pp. 81–86, doi: 10.4316/AECE.2013.01014
- [8] Polinder H., Hoeijmakers M.J.: 'Eddy-current losses in the permanent magnets of a PM machine'. 1997 Eighth Int. Conf. on Electrical Machines and Drives (Conf. Publication No. 444), Cambridge, UK, 1997, pp. 138–142, doi: 10.1049/cp:19971054
- [9] Eriksson S., Solum A., Leijon M., *ET AL.*: 'Simulations and experiments on a 12 kW direct driven PM synchronous generator for wind power', *Renew. Energy*, 2008, **33**, (4), pp. 674–681, doi: 10.1016/j.renene.2007.03.027
- [10] Eriksson S., Bernhoff H., Leijon M.: 'FEM simulations and experiments of different loading conditions for a 12 kW direct driven PM synchronous generator for wind power', *Int. J. Emerging Electr. Power Syst.*, 2009, **10**, (1), pp. 1–15, doi: 10.2202/1553-779X.1958
- [11] Rossander M., Goude A., Eriksson S.: 'Mechanical torque ripple from a passive diode rectifier in a 12 kW vertical axis wind turbine', *IEEE Trans. Energy Convers.*, 2017, **32**, (1), pp. 164–171, doi:10.1109/TEC.2016.2626783